IEEE Access
The journal for rapid open access publishing

IEEE Xplore Digital Library
http://ieeexplore.ieee.org/Xplore

Robust Authentication of Consumables with Extrinsic Tags and Chemical Fingerprinting

Naren Vikram Raj Masna, Cheng Chen, Soumyajit Mandal, and Swarup Bhunia

***Abstract*—Consumables - from food, to pharmaceuticals, and supplements - are becoming increasingly vulnerable to various modes of counterfeiting due to the growing complexity of their supply chain. Mislabeling, re-branding, and false advertising are prevalent in this sector. Existing physical authentication techniques fail to adequately verify integrity of these products and protect the end-users. In this paper, we aim at addressing this critical problem through development of a novel authentication solution. It builds on the chemical analysis properties of a powerful spectroscopy technique, namely, Nuclear Quadrupole Resonance (NQR), that is quantitative, non-invasive, low-cost, and amenable for miniaturization (to hand-held form factors). The method is sensitive to small variations in the solid-state chemical structure of a sample, which change the NQR signal properties. These attributes can be unique for various manufacturers, enabling their use as manufacturer-specific watermarks. However, NQR spectroscopy only works reliably (i.e., provides good sensitivity) on compounds that contain certain nuclear isotopes. We take advantage of the intrinsic properties of NQR-sensitive isotopes to use them as extrinsic tags in NQR-insensitive products. The NQR spectra of these extrinsic tags act as unique watermarks that can be analyzed using machine learning methods to authenticate any consumable with high confidence. In particular, we use support vector machines (SVMs) to classify the measured spectra and confirm the identity of items under test. We have assessed this approach on a variety of consumables utilizing semi-custom equipment, and verified that it results in high ($> 95\%$) classification accuracy. In order to prove the unclonability of such extrinsic tags, we have also performed a mathematical analysis that proves the randomness of the extrinsic tag and confirms its robustness to brute-force attacks.**

***Index Terms*—NQR, Authentication, Classification, Extrinsic Tagging, Consumables, Supply Chain.**

I. Introduction

TRUST is becoming an increasingly important factor in the life-cycle of consumables, from medicines to dietary supplements and diverse food products. This is primarily due to the complex and globally distributed nature of their supply chain, which often involves many untrusted parties at different stages – from manufacturing to distribution. Growing trends of online distribution of these products further aggravates the situation. According to a recent report, the value of food fraud amounts to approximately $40 billion a year globally [1]. Dietary supplements, which are commonly used by adults in many countries, are also highly prone to fraud. A study involving 37,958 adults found that 52% of them use at least one type of dietary supplement, while 31% use multiple supplements [2]. Current practices cannot provide adequate assurance of authenticity and safety of these products, particularly considering i) the rapid increase in their consumption - to an estimated $220.3 billion by 2022 [3]; ii) repeated reports claiming substandard control and storage [4]; and iii) insufficient oversight by regulators, such as the U.S. Food and Drug Administration (FDA) [5]. Similarly, essential medicines have been vulnerable to various types of fraudulent activities, with one out of 10 medicines in developing countries are falsified or substandard, according to the World Health Organization (WHO) [6]. For example, an incident in the city of Lahore, Pakistan, resulted in contamination of a drug with an antimalarial one leading to the death of 200 people [7]. Dominance of such fraudulent activities in variety of consumables is creating significant health concerns including death in many cases across the globe. There is a critical need to develop low-cost, reliable, and non-invasive authentication method for consumables to effectively track-and-trace them as they flow through the supply chain. Such a solution can also empower end-users to verify the products they consume.

Existing solutions, such as regulations for appropriate product labeling and package-level tagging, suffer from major deficiencies. While it is mandatory for manufacturers to provide a complete breakdown of the ingredients, there are few techniques available for authenticating the quality of these ingredients. Moreover, the globally distributed nature of the supply chain leads to the lack of communication and assignment of responsibility between involved parties. This provides opportunities for counterfeiters to enter into a supply chain, giving opportunity to various types of fraud. For example, the role of organized crime in food fraud came into light during a joint initiative named "OPSON V" by EUROPOL and INTERPOL in 2016, which resulted in the seizure of 11,000 tons of fake food and 1,440,000 liters of fake drinks across 57 nations [8]. Food and dietary supplement fraud happens in several ways, including (but not limited to) adulteration, use of low-cost substitutes, tampering, counterfeiting, mislabeling, and over-production. There is no centralized authentication method that covers the complete supply chain. Although some manufacturers use verification methods based on physical authentication techniques such as optical barcodes and radio frequency identification (RFID), they act only to verify the product information or labels on the package, which is easy to clone. They fail to verify the authenticity of the consumable substance inside a package.

In this paper, we present a novel, reliable, and effective authentication method for consumables by using embedded tags that provide unique chemical signatures based on nuclear quadrupole resonance (NQR) spectroscopy. As illustrated in Fig. 1, this approach allows a product to be authenticated at any stage of the supply chain using a portable NQR spectrometer and a computing device (e.g., a smart phone)

Digital Object Identifier: 10.1109/ACCESS.2019.2893518

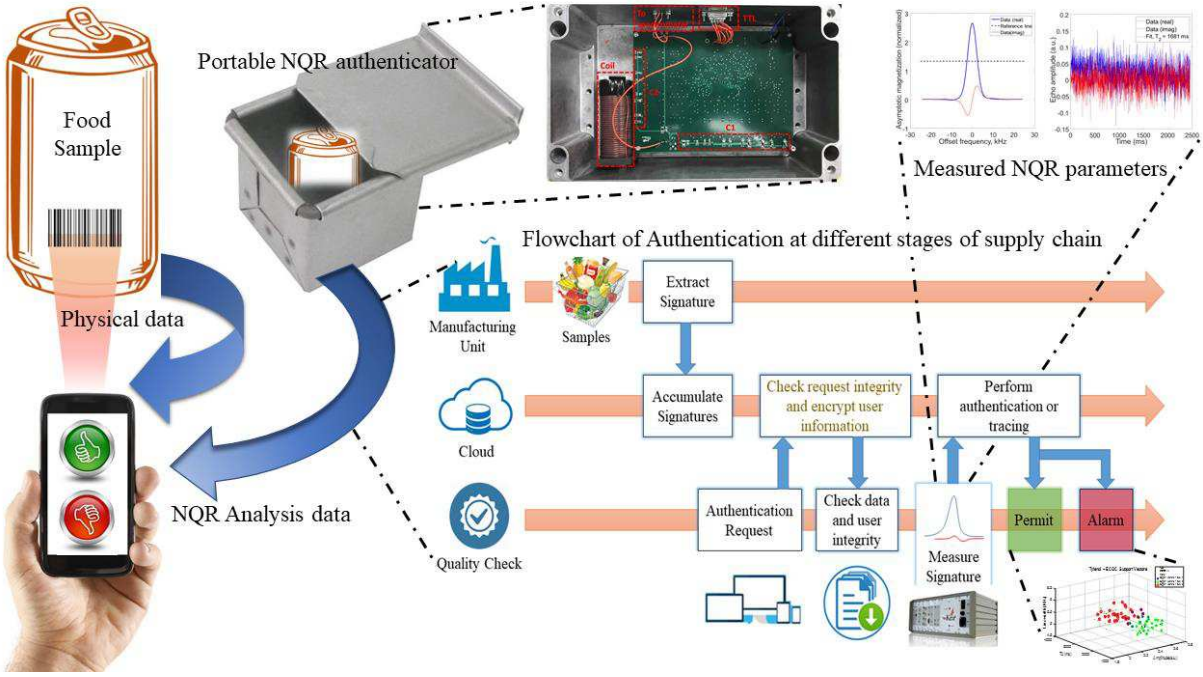

Fig. 1: Proposed authentication flow of a consumable product using NQR-based chemical tagging.

that runs a customized application. A manufacturer needs to store the NQR signatures of the ingredients being used for product authentication in a cloud server (preferably in encrypted form to avoid data theft) before forwarding the product to later stages in the supply chain. The cloud server can be used to protect and control the access of tag information from unauthorized users. It can also be used for defending against common attacks like eavesdropping and man-in-the-middle attacks. This integrity verification step can either be used to authenticate the product and/or to trace it back to a manufacturer. As the NQR signatures are extremely hard to duplicate (as explained in detail in Section V), the ingredients under test (known as chemical tags) can be used to check for different integrity issues, e.g., adulteration, mislabeling, and contamination. In case of authentication failure at any stage, the product can be brought to the attention of the manufacturer and/or regulatory authorities and appropriate measures can be taken. The proposed authentication method uses both intrinsic tags (explained in Section III) and extrinsic tags (explained in Section IV). The latter is used for consumables that are not sensitive to NQR. In such cases, we generate unique signatures based on the intrinsic properties of NQR-sensitive elements by embedding them in NQR-insensitive substances. The paper presents details on: i) approaches for embedding extrinsic tags, and ii) estimating their randomness and unclonability.

The remainder of this paper is organized as follows. Fundamentals of NQR-spectroscopy-based authentication, feature extraction, and machine-learning-based classification are explained in Section II. The experimental setup, NQR spectrum analysis, classification results using intrinsic material properties, and measurement accuracy are explained in detail in Section III. The concept of extrinsic tagging is introduced and analyzed in Section IV. The security of extrinsic tags, including their randomness functions, is analyzed in Section V. The results of the analysis and experiments are discussed in Section VI. Section VII concludes the paper and discusses future work.

II. Methodology

In this section, the physics behind the NQR and the process of extracting important parameters to create an authentication signature are explained. The basics of SVM classification and the concept of extrinsic tagging are also described.

A. Overview of NQR-based authentication

NQR spectroscopy is an analytical, quantitative, non-invasive, and non-destructive way to generate unique chemical signatures. It uses RF magnetic fields to generate and detect transitions between sub-levels of an atomic ground state [9], [10], [11]. These sub-levels are created by interactions between nuclear charge distributions and nearby electric field gradients (EFGs), and NQR spectra are a result of transitions between them [12], [10]. Nuclei with a spin of $I > 1/2$ embedded in a structure with lower than tetragonal symmetry produce NQR lines; in addition, high isotopic abundance results in increased sensitivity. NQR resonances occur in the RF range of the electromagnetic spectrum [13]. Unlike the closely-related analytical technique of nuclear magnetic resonance (NMR), NQR does not require a static external magnetic field to generate nuclear energy levels and transitions between them. Thus, NQR is also known as "zero-field NMR". The nuclear Hamiltonian relevant for NQR is given by

$$H_Q = \frac{\omega_Q}{3}\left[3I_z^2 - I(I+1) + \frac{\eta}{2}(I_+^2 + I_-^2)\right], \qquad (1)$$

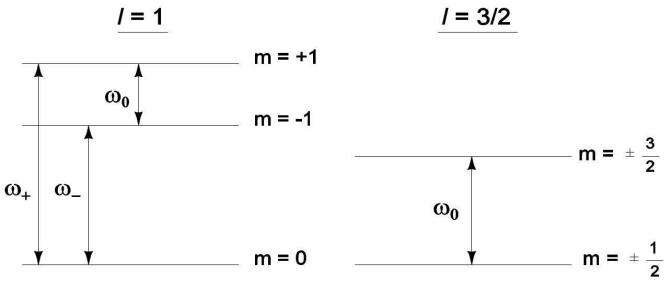

Fig. 2: Energy levels and transitions for quadrupolar nuclei with spin $I = 1$ and $I = \frac{3}{2}$. The three NQR resonant frequencies for $I = 1$ are denoted by ω_+, ω_-, and ω_0; the single resonant frequency for $I = 3/2$ is denoted by ω_0.

where ω_Q is the quadrupolar coupling constant, $0 \leq \eta \leq 1$ is the asymmetry parameter of the EFG tensor in the principal axis system fixed on the nucleus, and I_z, I_+, and I_- are spin operators. Fig. 2 shows the resulting stationary energy levels and transitions between them for nuclear spins $I = 1$ and $I = \frac{3}{2}$. In this paper, we focus on extrinsic tags based on detecting either nitrogen or chlorine. In particular, the ^{14}N isotope of nitrogen ($I = 1$) is chosen for many of the proof-of-concept experiments due to the widespread presence of nitrogen in food and dietary supplements, and also its high natural abundance (99.6%). However, the NQR resonances for ^{14}N occur at relatively low frequencies (0.1-5 MHz), which results in low sensitivity. Other nuclei such as ^{23}Na, ^{35}Cl, ^{37}Cl, and ^{39}K, all of which have $I = \frac{3}{2}$, can also serve as extrinsic tags; some of them (notably the chlorine isotopes) have significantly higher sensitivity than ^{14}N. The parameters ω_Q and η characterize the transition frequencies of a specific nuclear site. They depend upon the nearby electric field distribution, which is a sensitive function of molecular structure and chemical bonding.

B. Feature extraction from NQR spectra

In order to authenticate a substance, we need signatures that cannot be altered externally. We use NQR spectra to realize such unique signatures. NQR spectral lines occur at well-defined resonance frequencies in the RF range. Each spin $I = 1$ nucleus (e.g., ^{14}N) has three resonances, as predicted by eqn. (1):

$$\omega_\pm = \frac{3\omega_Q}{4}\left(1 \pm \frac{\eta}{3}\right), \quad \omega_0 = \omega_+ - \omega_- = \frac{\eta\omega_Q}{2}. \tag{2}$$

Similarly, each spin $I = 3/2$ nucleus (e.g., ^{35}Cl or ^{37}Cl), has a single resonance in the absence of an external magnetic field:

$$\omega_0 = \frac{\omega_Q}{2}\sqrt{1 + \frac{\eta^2}{3}}. \tag{3}$$

Thus, NQR resonance frequencies are functions of ω_Q and η, which are unique properties of molecular and crystal structure. Other properties of NQR spectra, such as amplitude (A) and line width (Δf), provide additional information on the molecule and the sample as a whole. For instance, the amplitude is proportional to concentration of the active ingredient, while the line width varies with crystal structure, disorder, stress, aging, and other factors [14], [15], [16]. Thus, these parameters are sensitive functions of solid-state structure, which enables us to obtain unique signatures from NQR spectra.

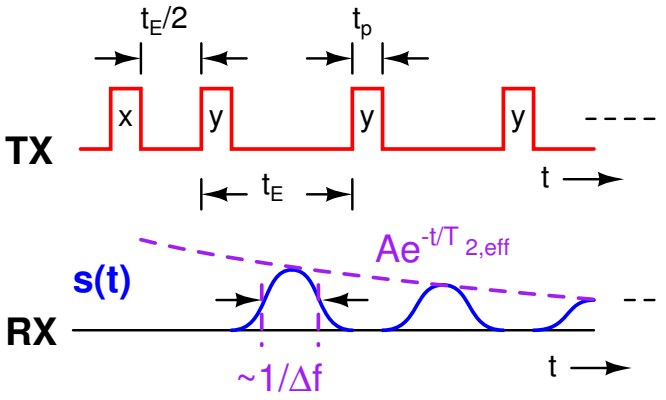

Fig. 3: SLSE pulse sequence used in NQR experiments and the corresponding received signal $s(t)$.

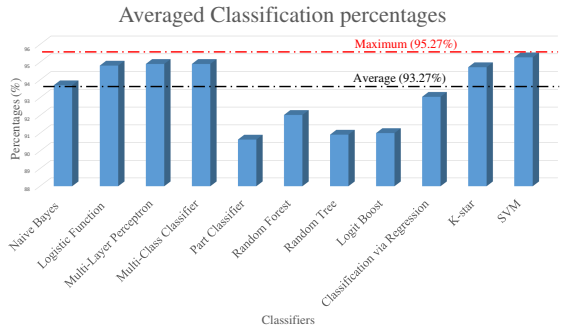

Fig. 4: Average accuracy of different classification algorithms using the intrinsic properties of three samples: acetaminophen, L-Histidine, and L-Proline [19].

We use pulsed measurements to rapidly measure NQR spectra. In particular, we use the spin-locked spin echo (SLSE) sequence [17], [18], which comprises of an initial excitation pulse and a long train of refocusing pulses separated by fixed echo periods (see Fig. 3). Both the excitation and refocusing pulses have the same length and a relative phase shift of $\pi/2$ between them. NQR signals known as spin echoes (indicated as $s(t)$ in Fig. 3) form between the refocusing pulses. Nonlinear fitting is used to extract three main parameters from these echoes: initial amplitude (A), frequency domain line-width (Δf), and decay time constant ($T_{2,eff}$). Note that $1/(\Delta f)$ is roughly equivalent to the width of each echo, which is substantially smaller than $T_{2,eff}$. These NQR parameters provide sample-specific information, i.e., act as chemical fingerprints, and are thus used as features for classification.

C. SVM-based classification

Given a list of training samples with NQR parameters (A, $T_{2,eff}$, and Δf) as predictors, every signature defines one class - namely, the manufacturer. We have extensively

studied the performance of various classification algorithms on these features. Our results, which are summarized in Fig. 4, suggest that SVMs have the best overall performance (highest classification accuracy). Thus, they were selected for our experiments on the authentication of consumables. The basic SVM algorithm can be understood by considering data as points in M-dimensional space, where M is the number of parameters ($M = 3$ in our case). The algorithm finds the classification boundary that separates two training sets by the largest possible margins; the data points situated on the margins are known as support vectors. This results in a non-probabilistic binary classifier. It is combined with an error-correcting output codes (ECOC) classifier to build a multi-class model that assigns new data to one of the manufacturers in the training database. The trained classifier can be used to test samples at any stage of the supply chain for verification and traceability. Additionally, by checking the investigation log of each stage, changes in classifier estimates can be used to infer fraud or degradation.

III. Analysis of Intrinsic Properties

A. Experimental setup

The experimental setup comprises of an inductive detector (solenoid coil) and programmable impedance matching network mounted inside a Faraday cage to decrease environmental radio frequency interference (RFI). The matching network is connected to a commercial bench-top magnetic resonance (MR) spectrometer (Kea2, Magritek) that contains a power amplifier (PA), low-noise amplifier (LNA), and transmit-receive switch (duplexer). The PA works as the transmitter and the LNA as the receiver, while the duplexer switches the coil and matching network amongst transmit and receive modes. The spectrometer is powered by two 12 V, 18 Ah lead-acid batteries connected in series. It is controlled from a PC via a graphical user interface (GUI) named Prospa that enables the user to create pulse sequences and store the acquired data [17], [18].

One of the important parts of the setup is the sample holder, on which the solenoid coil is wound. This is utilized for both excitation and detection, i.e., by creating a RF magnetic field that generates transitions between the nuclear energy levels in transmit mode, and inductively detecting the subsequent time-varying magnetic flux in receive mode. Our coil was created by winding AWG 20 wire around a hollow PVC tube of height 90 mm and base diameter 30 mm; the external surface of the tube is threaded to hold the coil. We use a design with 31 turns, an effective diameter of 31 mm, and a length of 70 mm. The solenoid is then safely mounted inside the Faraday cage (size $= 260$ mm $\times$ 160 mm $\times$ 90 mm), which minimizes RFI and also houses the matching network [20]. The latter is tuned to a particular frequency by utilizing TTL-level digital signals from the spectrometer that assign "on" and "off" states to capacitor channels (see Fig. 5).

The tuning procedure is as follows: The spectrometer creates a programmable number of sequential pulses. These pulses are counted by an accumulator on the matching network board. The output bits of the accumulator define a binary code that is used to switch the states of individual capacitors,

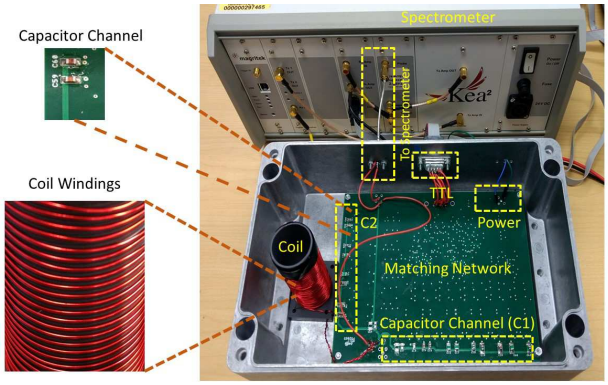

Fig. 5: Setup used for ^{14}N NQR experiments.

thus programming the matching frequency. The programming time is constrained by the number of programming pulses, e.g., for $n = 10$ channels, the highest possible number is $2^n - 1 = 1023$. We decreased this time by utilizing base-$n/2$ notation, i.e., dividing the sequence into two signals, each of which programs only $n/2 = 5$ channels. This reduces the highest possible number of pulses to $2(2^{n/2} - 1) = 62$, thus minimizing the programming time by $\sim 16\times$.

B. Parameter estimation and SVM classification

The impact of environmental variables like temperature on the measurements can be critical. The proposed approach requires the analysis to be stable across different measurements. Appropriate design of the device and calibration procedures are essential to minimize these effects. In our previous work, we used a combination of in-built temperature sensors with pre-computed calibration tables to remove temperature-driven NQR measurement variations [19]. In this work, we used the intrinsic NQR properties of three substances for classification, namely acetaminophen (Tylenol), L-histidine, and L-proline. The first is a typical over-the-counter medicine, while the others are amino acids that are frequently consumed as dietary supplements. Each of these substances contains one or more ^{14}N atoms, and are thus NQR-active. For each substance, we prepared samples with similar amounts of active ingredient from three different manufacturers.

Typical experimental data is shown in Fig. 6. The acquired echoes are i) processed by a matched filter to maximize signal-to-noise ratio (SNR), and then ii) fit to a mono-exponential decay function to evaluate $T_{2,eff}$ (see Fig. 6(b)). The value of $T_{2,eff}$ can vary from a few milliseconds to several seconds, depending on the sample; larger values require longer measurement times. Also note that while mono-exponential decay curves fit this specific data set, in many cases the decays are bi-or multi-exponential, which would increase the number of classification parameters. Signal amplitude is estimated as the peak value of the spectrum (see Fig. 6(a)) while line-width is measured at 50% of the peak amplitude (see Fig. 6(c)). Since the SLSE sequence acquires the signal in pulse mode, rather than estimating the genuine line-width of the example, we are actually estimating it after convolution with the Fourier transform of the acquisition window. Fortunately, this only

TABLE I: Measured ECOC-SVM prediction accuracies for some consumables.

	Tylenol	L-histidine	L-proline
Re-substitution accuracy	95.00%	97.50%	97.80%
Cross validation accuracy	94.36%	96.70%	93.33%

adds a constant offset to the measured line width and does not influence the classification results. If needed, this effect can be numerically reduced by deconvolution.

The presence of noise in the measurements (i.e., the finite SNR) results in parameter estimation errors. Fig. 7 shows an example of the distributions of estimated parameter values for various samples across multiple experimental runs. For a given experiment, the parameter distributions can be estimated using a bootstrapping-like procedure, as described in the next section. These distributions can in turn be used to estimate the statistical significance of the measurements (e.g., using confidence intervals).

3D scatter plots showing the intrinsic parameters of the products under test are shown in Fig. 8. The corresponding support vectors are also shown. The three measured parameters were used to train a SVM-ECOC model for multi-class classification. Its performance was assessed using re-substitution response prediction accuracy and cross validation accuracy, and good results were obtained as summarized in Table I. The term "re-substitution" refers to the accuracy achieved by a trained classifier on the training set. It is known that re-substitution accuracy is positively biased; hence cross-validation is a more suitable technique for predicting the performance of the trained classifier on test sets.

C. Statistical significance of the measured parameters

NQR is a relatively insensitive method because of the small differences between the nuclear energy levels, which results in low resonance frequencies (0.1-5 MHz for ^{14}N). Thus, it is important to ensure that SNR is high enough to enable statistically significant measurements of sample properties. In addition to intrinsic noise sources like thermal noise in the detector, NQR is as also vulnerable to i) external RFI such as AM radio stations, and ii) environmental perturbations such as temperature fluctuations. We use temperature control and RF shielding to minimize these error sources, but active noise cancellation using multiple detectors [21] can also be used.

Here we describe a bootstrapping-like approach for evaluating i) the statistical properties of our parameters in the presence of noise sources, and ii) the resulting false positive and false negative rates. Our approach is to repeat the fitting procedure many times with artificially-generated synthetic noise that has similar statistics (mean and standard deviation) as the experimental noise. Signal parameters (A, Δf, and $T_{2,eff}$) are estimated at the end of each test, and their statistics are examined to assess measurement uncertainty.

The assessment procedure proceeds as follows: i) weigh the measured signals (echoes) by their anticipated amplitudes utilizing an initial estimate of $T_{2,eff}$; ii) matched filter the echoes; and iii) fit to an exponential decay function to get the values of A and $T_{2,eff}$. The residuals from the fit provide an approximation to the noise, and are used to generate synthetic noise waveforms. These are added to the fitted decay curve and fed back to the fitting routine to obtain new estimates for the signal parameters. The distributions of these parameters can be visualized using histograms, as shown in Fig. 9. These are approximately Gaussian when external noise sources are absent, since the intrinsic noise of the detector is approximately additive, white, and Gaussian. These distributions allow us to i) estimate the number of scans and total experimental time required to obtain the desired level of precision (e.g., specified false positive and false negative rates); and ii) recognize and eliminate statistical outliers, i.e., measurements for which the noise statistics fall outside the expected range due to external RFI or instrumentation issues.

D. Statistical significance of SVM-ECOC classifiers

The statistical significance of the trained SVM-ECOC classifiers was validated using permutation testing (10,000 iterations). Permutation or randomization testing is a statistical tool for constructing sampling distributions [22]. Specifically, it consists of i) permuting the collected data by assigning random outcome values to each observation from among the set of possible outcomes, and ii) evaluating the prediction accuracy of the trained classifier on the permuted data. This procedure is similar to bootstrapping, except for the fact that it is carried out with replacement.

Permutation tests are particularly useful in experimental studies, where we often wish to eliminate the null hypothesis of no significant difference between the classification groups. In these situations, the permutation test represents our process of inference, because our null hypothesis is that the two treatment groups do not differ on the outcome as they are manually modified. When we permute the outcome values during the test, we therefore obtain all the possible alternative treatment assignments. While the procedure actually requires that we test all possible permutations of the data, We can easily conduct "approximate permutation tests" by simply conducting a very large number of re-samples. That process should approximate the actual permutation distribution.

The probability distribution of classification accuracy for the null distribution of the consumables under test is nearly Gaussian with a mean of 42% and a standard deviation of 3.35%. This is statistically distinct (at the 16σ level) from the cross validation accuracy of 97.5% obtained from one of the correctly-labeled data sets (see Fig. 10). This result proves that the prediction accuracy obtained by cross-validation and re-substitution cannot be obtained from random data.

E. Variations with manufacturing processes

The linewidth of NQR spectra varies with the manufacturing process [23], [24]. Similar NQR-sensitive substances with the same polymorphic form have different linewidths when they are made at different facilities. The narrowest linewidths occur for single crystals, followed by free powder forms. By contrast, the linewidth broadens as pressure is applied to convert free powder into pill form.

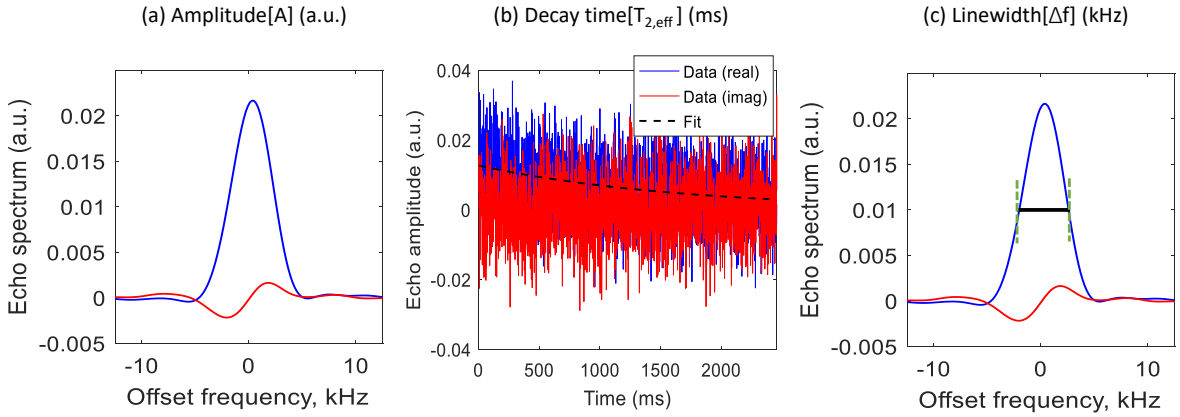

Fig. 6: Measured ^{14}N NQR parameters of a typical compound, namely acetaminophen. Experimental conditions: RF frequency = 2.564 MHz, inter-experimental delay = 3000 ms, pulse length = 200 μs, echo period = 1200 μs, number of echoes = 2048, number of scans = 16, number of pills = 50 (500 mg each).

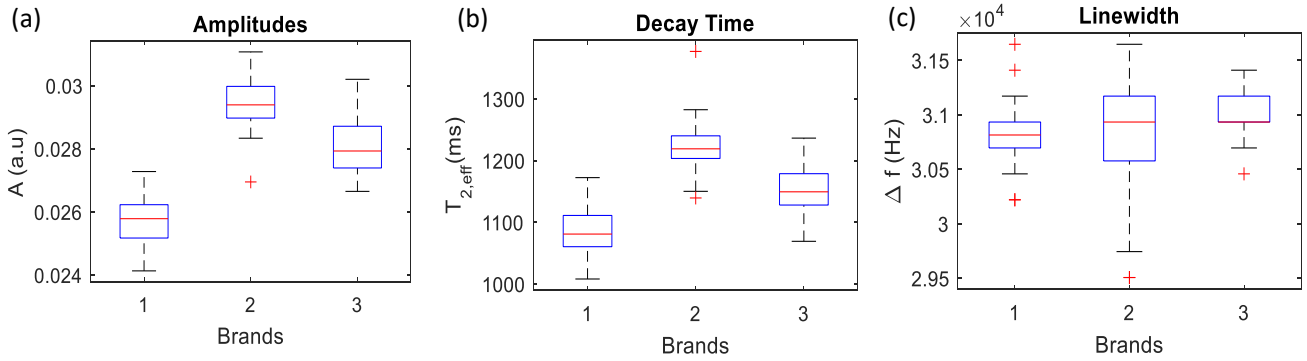

Fig. 7: Comparison of the measured distributions of the NQR parameters for three different brands of L-Histidine. Experimental conditions: RF frequency = 2.390 MHz, inter-experimental delay = 2000 ms, pulse length = 200 μs, echo period = 1200 μs, number of echoes = 2048, number of scans = 16, number of pills = 30 (500 mg each).

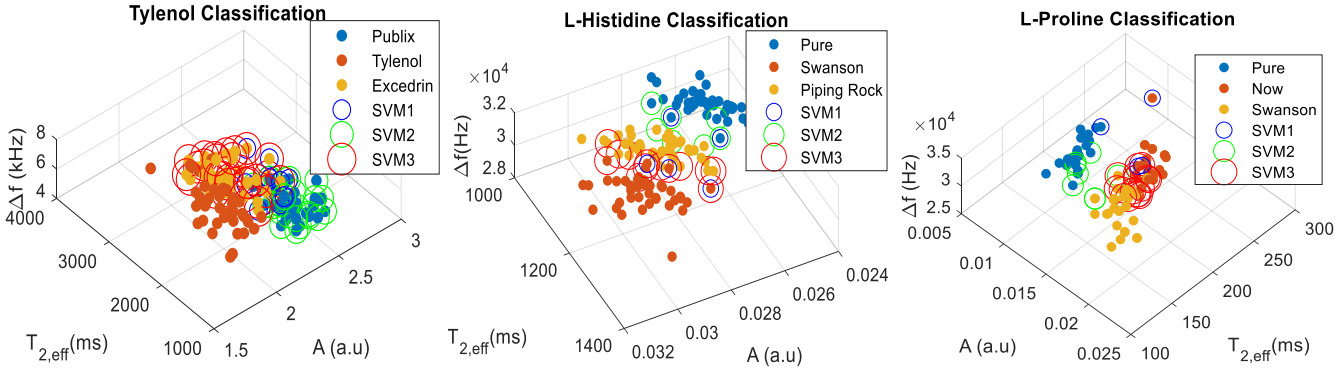

Fig. 8: SVM classification with ECOC support vectors of three different samples using their intrinsic NQR signatures. The classification accuracies are shown in Table I. RF frequencies: Tylenol = 2.564 MHz; L-histidine = 2.390 MHz; L-proline = 1.490 MHz. Quantities: Tylenol = 50 pills (500 mg each); L-histidine = 30 pills (500 mg each); L-proline = 30 pills (500 mg each).

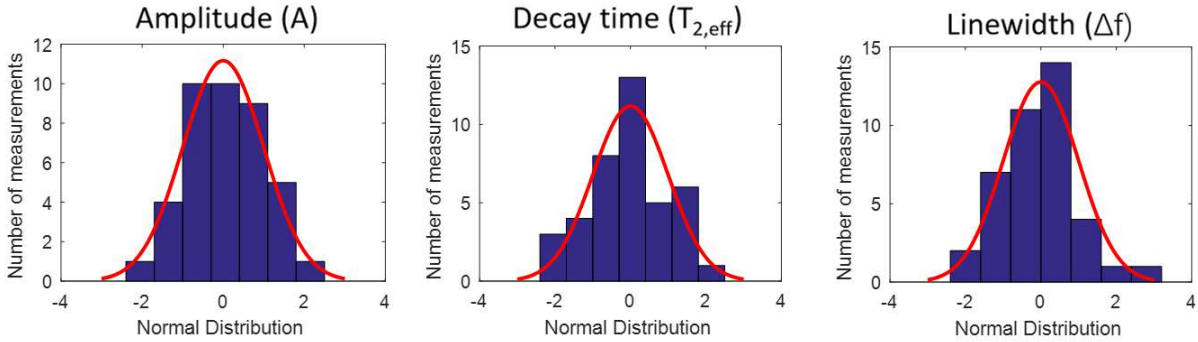

Fig. 9: Histograms of the measured parameters for one brand of acetaminophen obtained using the bootstrapping-like procedure. Gaussian fits to the histograms are also shown. Experimental conditions: RF frequency $= 2.564$ MHz, inter-experimental delay $= 3000$ ms, pulse length $= 200$ μs, echo period = 1200 μs, number of echoes $= 2048$, number of scans $= 16$, number of pills $= 50$ (500 mg each).

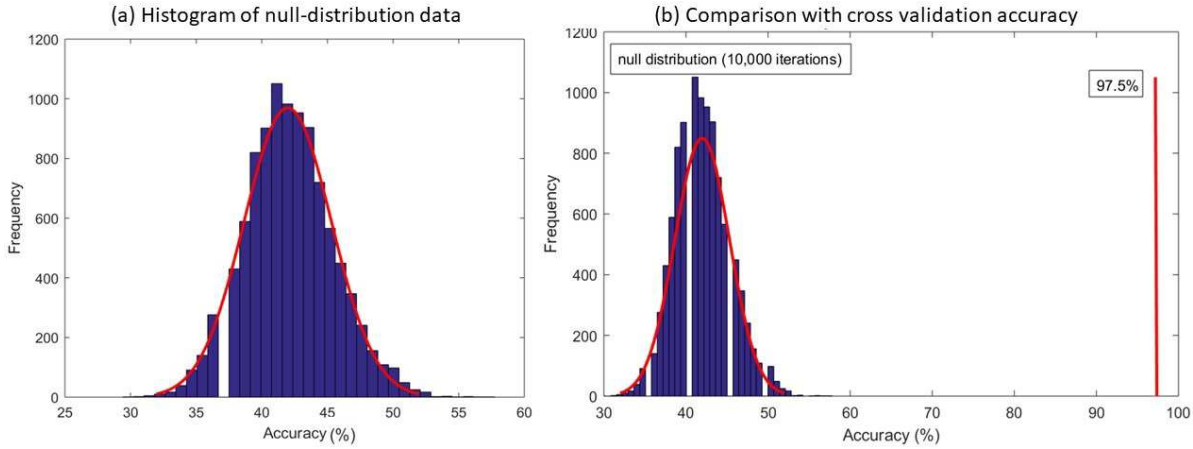

Fig. 10: Statistical significance of the SVM-ECOC classifier using permutation testing. The classifier was trained on the acetaminophen data shown in Fig. 9.

To test this hypothesis, we used a pill press to prepare custom pills from mixtures of L-histidine and different excipients. The customized pills contained pure L-Histidine (80-90% by mass) and suitable excipients (fillers, binders, and glidants). In particular, we used a binding agent as the excipient to prepare custom pills with a diameter of 8 mm (similar to commercially-available ones). The NQR spectra of both the powder and pill samples around 2.39 MHz were then measured. Statistically significant changes in the linewidth were observed, as shown in Fig. 11. In particular, there is a change of approximately 10σ in the linewidth, which is presumably because the high pressure applied during pill preparation physically deforms the crystal structure.

IV. Extrinsic Tagging

We refer to signatures generated using features of NQR spectra as the *intrinsic tags* of that particular nucleus in the sample. Obviously, intrinsic tags are only available for NQR-sensitive nuclear isotopes. The use of these features to create robust signatures for NQR-insensitive substances is known as *extrinsic tagging*. The general concept of extrinsic tagging is common in the fields of medicine and chemistry; it is used in metabolic incorporation, ingestible medicines, and for labeling proteins. Such tags are added to the original substance for analysis, signature generation, and labeling without affecting native performance. A common example is the study of protein function in living organisms by selective labeling through genetic encoding of fluorescent tags that enable high-resolution imaging [25]. Similarly, RF transponders as extrinsic tags attached directly to the outer surface of a standard-sized capsule can potentially serve as a cost-effective method of validating medication compliance via electronic detection of ingested pills inside the digestive tract [26]. Likewise, in our approach, in addition to intrinsic tags that generate signatures from existing ingredients of the material under test, we can add extrinsic tags to NQR-insensitive materials. As the proposed SVM-based ECOC classification approach has high prediction accuracy when trained using the intrinsic NQR parameters of NQR-sensitive products [19], we use the same concept to identify the extrinsic tags. Extrinsic tags should not i) chemically react with the original substance, or ii) affect its primary functions. Thus, the best practice for making extrinsic tags is to physically mix them with the substance to be tagged during manufacturing (e.g., injection molding or 3-D printing).

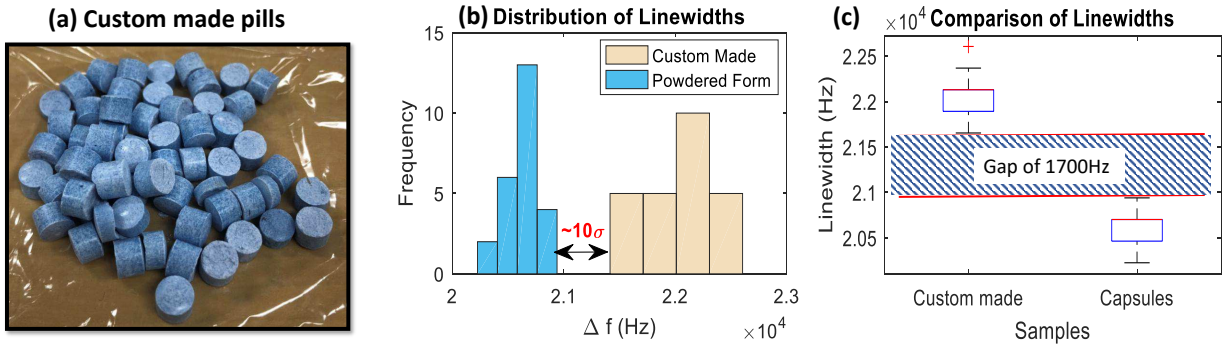

Fig. 11: Analysis of variations in linewidth between L-histidine in two physical forms: custom pills and powder. Experimental conditions: RF frequency = 2.390 MHz, inter-experimental delay = 2000 ms, pulse length = 200 μs, echo period = 1200 μs, number of echoes = 2048, number of scans = 16.

Moreover, enough tagging material should be added to enable accurate signature readout within a reasonable period time. This section further describes the extrinsic tagging concept.

A. Toxicity

In food applications, the chosen extrinsic tag will be consumed directly by the consumer along with the product, which limits the choice of tagging compounds. We select extrinsic tags that are directly or indirectly safe to consume based on a database available from the Food and Drug Administration (FDA) [27]. Moreover, the tag should not i) chemically react with the material being tagged, or ii) significantly change the physical or sensory properties (e.g., color, taste, smell, etc.) of the product. There are two main options that satisfy these requirements: i) dietary supplements (which are directly consumable) detected using ^{14}N NQR; ii) other compounds (which may be directly or indirectly consumable) detected using NQR of various nuclei such as ^{14}N, ^{23}Na, ^{27}Al, ^{35}Cl, ^{39}K, ^{55}Mn, ^{67}Zn, and ^{127}I. Table II lists some compounds in the latter category that have potential as extrinsic tags for consumables.

B. Optimizing the signal-to-noise ratio (SNR)

In this section, we analyze the duration of a tagging experiment. As NQR has relatively poor sensitivity, single-scan signals are usually too weak to reliably detect. Thus, a common approach is to average more scans to reduce the noise, resulting in an improvement of the SNR. Specifically, if the noise is uncorrelated across scans, the SNR after accumulating N scans increases by $\sqrt{N}$ (in voltage units). We can obviously keep extending the experiment time to get better SNR, but in most cases, we hope that the experiment is not only effective but as short as possible. Thus, we wish to maximize the SNR per unit time, which we denote by SNR$_t$. We now derive general expressions for maximizing SNR_t for a given sample. Assuming a mono-exponential decay for simplicity, the total NQR signal strength (obtained by adding the acquired echoes) after one scan is given by

$$S_{tot} = \sum_{n=1}^{N_E} A e^{-nT_E/T_{2,eff}}, \tag{4}$$

TABLE II: Potential extrinsic tags for food and dietary supplements.

Type	Name	Formula	Nuclei	Freq. (MHz)
Directly consumable	Ammonium chloride	NH_4Cl	N-14, Cl-35	Cl: 20-40
	Calcium chloride	$CaCl_2$	Cl-35	Cl: 20-40
	Calcium iodate	$Ca(IO_3)_2$	I-127	I: 40-80
	Manganese chloride	$MnCl_2$	Mn-55, Cl-35	Cl: 20-40
	Potassium chloride	KCl	K-39, Cl-35	Cl: 20-40
	Potassium iodide	KI	K-39, I-127	I: 40-80
	Pyridoxine hydrochloride	$C_8H_{11}NO_3$ HCl	Cl-35	Cl: 20-40
Indirectly consumable	Sodium chlorite.	$NaClO_2$	Cl-35	53.502, 51.121,
Nutrients	Zinc oxide.	ZnO	Zn-67	0.7220 0.3610
Multi-purpose food items	Glutamic acid hydrochloride.	$C_5H_{10}ClNO_4$	Cl-35, N-14	Cl:20-40
	Aluminum sodium sulfate.	$NaAl(SO_4)_2 \cdot 12H_2O$	Na-23, Al-27	Na:1-3, Al:1.5-2
Anti-caking agents	Sodium aluminosilicate.	$AlNa_{12} \cdot SiO_5$	Na-23, Al-27	Na:1-3, Al:1.5-2
Chemical preservatives	Sodium sulfite.	Na_2SO_3	Na-23	Na:1-3
Nutrients	Choline chloride.	$C_5H_{14}ClNO$	Cl-35, N-14	Cl:20-40

where A is the initial signal amplitude, T_E is the echo time, N_E is the number of echoes, and $T_{2,eff}$ is the transverse relaxation time constant. Two scans are separated by a wait period T_W, during which the available signal amplitude recovers exponentially as $\left(1 - e^{-T_W/T_1}\right)$, where T_1 is the longitudinal relaxation time constant.

Thus, the SNR per unit time (in power units) is given by

$$SNR_t = \frac{{S_{tot}}^2 \left(1 - e^{-T_W/T_1}\right)^2}{(N_E T_E + T_W)} \frac{1}{N_E \sigma_{noise}^2}, \tag{5}$$

where T_W is the wait time and σ_{noise} is the rms noise per echo per scan (assumed to be additive and white, i.e., uncorrelated between echoes and scans).

For simplicity, we define the parameters $\beta = N_E T_E / T_{2,eff}$, $\alpha = T_W / T_1$, and $\delta = T_1 / T_{2,eff}$. Thus, eqn. (5) becomes

$$SNR_t = \frac{A^2}{\sigma^2_{noise}} \left(\frac{1 - e^{-\beta}}{1 - e^{-T_E/T_{2,eff}}} \right)^2 \frac{\left(1 - e^{-T_W/T_1}\right)^2}{N_E (N_E T_E + T_W)}. \quad (6)$$

Taking advantage of the approximation $\frac{1}{1-e^{-x}} \sim \frac{1}{x}$ when $x = T_E / T_{2,eff} \ll 1$, eqn. (6) can be rewritten as

$$SNR_t = \frac{A^2}{\sigma^2_{noise}} \frac{1}{T_E} \frac{(1 - e^{-\alpha})^2 \left(1 - e^{-\beta}\right)^2}{\beta(\beta + \alpha\delta)} = \frac{\gamma A^2}{S_{noise}} \frac{(1 - e^{-\alpha})^2 \left(1 - e^{-\beta}\right)^2}{\beta(\beta + \alpha\delta)}, \quad (7)$$

where S_{noise} is the power spectral density (PSD) of the noise. The noise PSD is defined using $\sigma^2_{noise} = S_{noise} \Delta f$ where Δf is the effective bandwidth of each echo after matched filtering. Also, we define $\gamma = 1/(\Delta f T_E)$ to be another dimensionless parameter. For pulsed measurements such as the SLSE sequence, $\Delta f \approx (1/T_2^* + 1/T_{acq})$ where $1/T_2^*$ is the line width and T_{acq} is the duration of the signal acquisition window for each echo. Clearly $T_{acq} < T_E$ since signals cannot be acquired during the RF pulses; as a result, $0 < \gamma < 1$.

Eqn. (7) shows that the SNR per unit time depends on various parameters. Of these, i) α and β depend on the pulse sequence parameters $N_E T_E$ and T_W; ii) γ increases monotonically with T_{acq}/T_E and is limited by hardware constraints (peak RF power level, duplexer isolation, etc.); iii) A and δ only depend on sample properties, and iv) S_{noise} is limited by the receiver hardware (i.e., coil resistance and Noise Figure [NF]). We can thus estimate the optimum pulse sequence parameters for a given instrument and sample by numerically evaluating the nonlinear function shown in eqn. (7) versus α and β for fixed values of A, S_{noise}, γ, and δ.

Fig. 12(a) shows the normalized SNR per unit time function for $\delta = 3$. A clear optimum is obtained near $(\alpha, \beta) = (1.57, 0.98)$. Fig. 12(b) summarizes the optimum values of α and β as a function of δ. As δ increases, i.e., T_1 becomes relatively larger than $T_{2,eff}$, it becomes more favorable to acquire echoes rather than wait increasingly longer times for T_1 relaxation. Thus, the optimum value of α decreases with δ, while that of β increases. However, the dependence of α_{opt} and β_{opt} on δ is relatively weak.

As an example, Fig. 13(a) shows the dependence of SNR per unit time on $N_E T_E$ and T_W for ^{35}Cl NQR of sodium chlorate ($NaClO_3$), for which the nominal values of T_1 and $T_{2,eff}$ at room temperature are 31 ms and 5 ms, respectively. Fig. 13(b) confirms that the experimentally measured SNR per unit time for $NaClO_3$ is in agreement with the theory, i.e., reaches an optimum for a given value of T_W when the scan time $N_E T_E$ is kept fixed. We created a modified version of the ^{14}N test setup shown in Fig. 5 for this experiment; this version uses a smaller sample coil and higher-frequency matching network such that ^{35}Cl NQR lines (which occur in the 20-35 MHz range) can be measured.

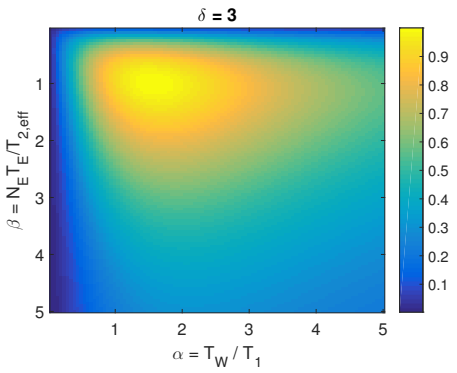

(a)

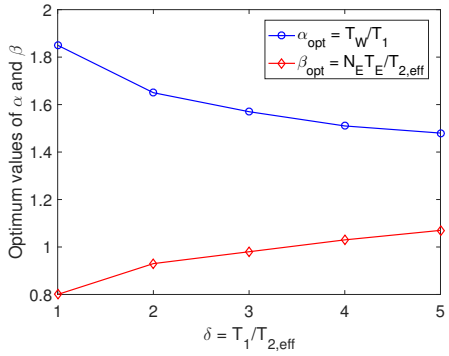

(b)

Fig. 12: (a) Theoretical dependence of SNR per unit time on α and β for $\delta = 3$. (b) Theoretical dependence of the optimum values of α and β as a function of δ.

C. Sensitivity

Sensitivity plays a major role in choosing an extrinsic tag as it directly determines the SNR per unit amount of tagging material. NQR signal strength scales as the square of the resonant frequency ω_0, so compounds with high resonance frequencies are desirable [18]. As a result, the amount of NQR-sensitive tag that can be reliably detected within a specified detection period depends on the tag. As an example, we limited the detection time to a maximum of 40 sec, used the optimum pulse sequence parameters derived in the previous section, and then evaluated the minimum amount of active ingredient required for reliable detection of L-histidine and L-proline. It should be noted that these compounds have low ^{14}N resonance frequencies of 2.39 MHz and 1.48 MHz, respectively. Hence the amount of tag required is relatively large. In our case, we can reliably detect changes in concentration of an L-histidine tag (in powder form) at the 10% level within a $\sim$50 cm^3 sample. For example, Fig. 15 shows that we can reliably classify samples of common sugar containing 30% and 40% of L-histidine. Thus, the estimated sensitivity (within the specified 40 sec detection time limit) for this tag is $\sim$5 cm^3, which corresponds to $\sim$2.1 gm of powder. Of course, averaging across more scans will further improve sensitivity as the square root of detection time.

Sensitivity can be greatly improved by using tags with higher resonant frequencies, as mentioned earlier. However, the improvement is not quite quadratic with ω_0 because of two factors: i) the power spectral density of noise in the detector coil increases due to proximity and skin effects; and ii) the

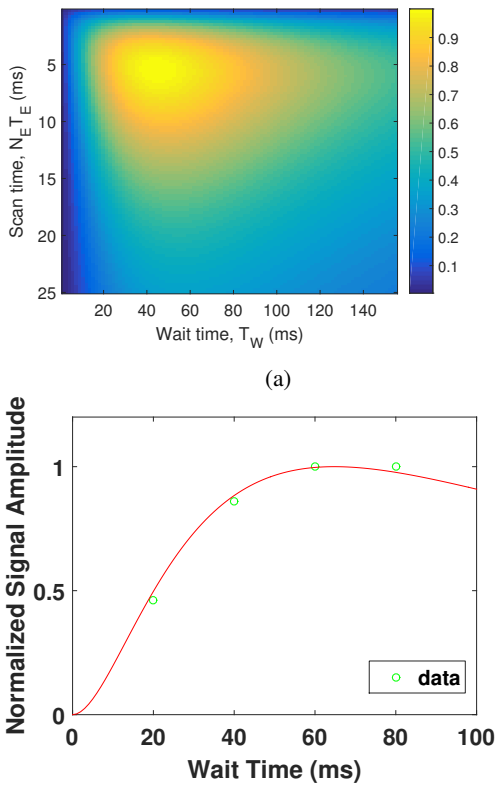

(a)

(b)

Fig. 13: (a) Theoretical dependence of SNR per unit time on wait and scan times for sodium chlorate ($NaClO_3$). (b) Comparison of theoretical and experimentally measured dependence of SNR per unit time (in this case, proportional to the acquired signal amplitude per unit time) on wait time T_W for $NaClO_3$ when the scan time $N_E T_E$ was fixed at 6 ms.

NQR line width also tends to increase, which increases the noise bandwidth. Assuming that i) the skin effect is dominant and ii) the line width is proportional to ω_0, it can be shown that the resulting sensitivity scales as $\omega_0^{5/4}$, i.e, increases in a roughly linear way with ω_0. The resonant frequencies of ^{35}Cl, for example, often lie in the 20-35 MHz range, which results in $\sim$20$\times$ higher sensitivity than typical ^{14}N resonances in the 1.8-3.2 MHz range. This allows smaller amounts of tag to be added to the material of interest.

We have used sodium chlorate, which has a resonant frequency around 29.91 MHz at room temperature, as an example of ^{35}Cl-based tagging. In particular, we have measured samples with different quantities of sodium chlorate; the results are shown in Fig. 14. The figure shows that this ^{35}Cl-based tag can be reliably identified in extremely low quantities (0.1 g within $\sim$40 sec, which is $\sim$20$\times$ better than the L-histidine ^{14}N-based tag, as expected). Furthermore, the signal strength is linearly proportional to the sample weight, which proves the quantitative nature of NQR. The large variance of the 0.9 g sample is due to the inhomogeneity of the detection coil and temperature shift during the experiment.

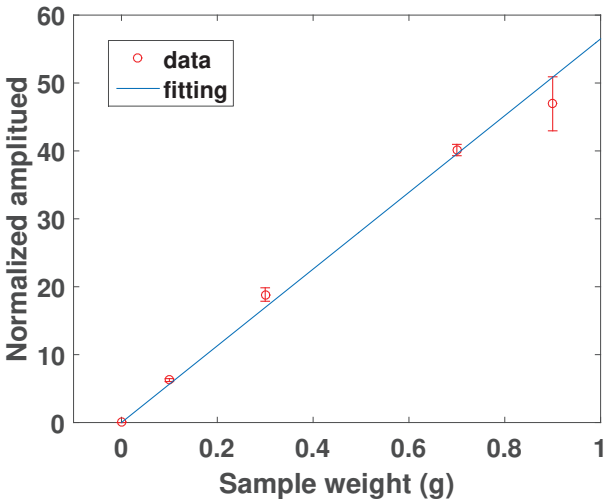

Fig. 14: High sensitivity of a sodium chlorate tag. Experimental conditions: RF frequency = 29.91 MHz, inter-experimental delay = 200 ms, pulse length = 50 μs, echo period = 600 μs, number of echoes = 100, number of scans= 128.

V. Complexity Analysis

Computational complexity of the deployed algorithm plays an important role in the practical implementation of the technique, since it determines the hardware requirements. We have estimated the computational complexity of SVMs during both the training and prediction phases. The training complexity of nonlinear SVMs is generally between $O(n^2)$ and $O(n^3)$ where n is the number of training instances [28]. We used a maximum of 40 instances and 3 features for training an SVM on each sample, which resulted in $> 90\%$ accuracy as described earlier. Similar training datasets can thus be used for commercial applications of the technique. Given the computational power of modern machines, training on such datasets only takes a few seconds. For example, in our case training took 6.8 sec using MATLAB running on a standard laptop computer (64-bit operating system, Intel-i7 8550U CPU). Similarly, the prediction complexity of a SVM is also low: it scales as $O(d)$ where d is the number of dimensions or features [29]. In our case, the same laptop took 4.6 sec to complete the prediction task given 3 features and a test dataset consisting of 34 samples.

Extrinsic tags should be difficult to clone to ensure high security. Tags with complex NQR spectra generated by several intrinsic or external NQR-sensitive nuclei are therefore desirable. There are several ways to make the extrinsic tag unclonable. Since we use three parameters from each NQR resonance for classification, we can permute these parameters in several combinations to make it extremely difficult for the attacker to guess them by brute force attacks. To further study the properties of extrinsic tags, we performed several experiments by modifying the parameters and also by using multiple tags. These are explained in the following sections.

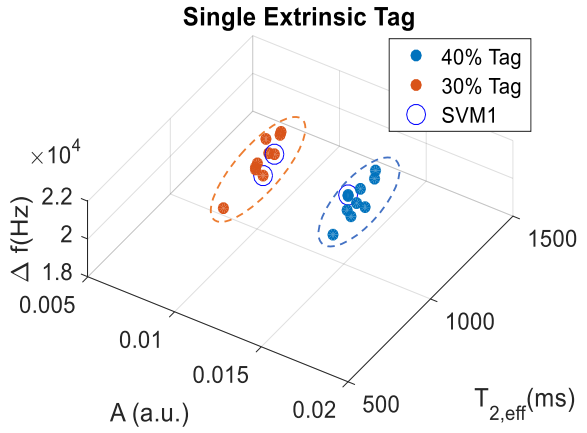

Fig. 15: Classification of two samples of common sugar using a single extrinsic L-histidine tag. Experimental conditions: RF frequency = 2.390 MHz, inter-experimental delay = 2000 ms, pulse length = 200 μs, echo period = 1200 μs, number of echoes = 2048, number of scans = 16.

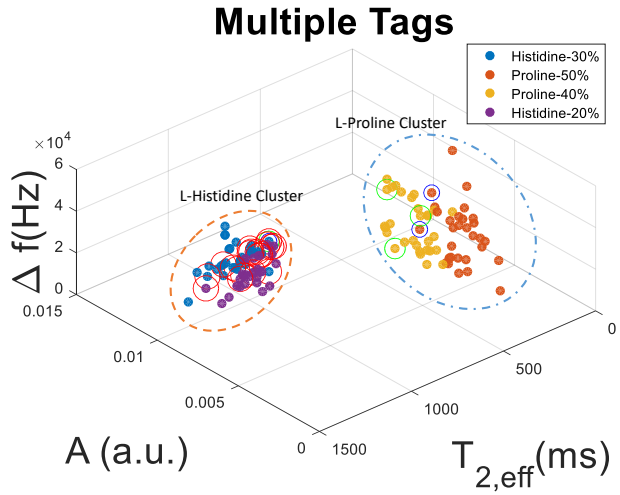

Fig. 16: Classification of two samples of milk powder using multiple extrinsic tags (L-histidine and L-proline). Experimental conditions: RF frequency = 2.390 MHz (L-histidine); 1.490 MHz (L-proline), inter-experimental delay = 2000 ms, pulse length = 200 μs, echo period = 1200 μs, number of echoes = 2048, number of scans = 16.

A. *Single extrinsic tag*

One of the important parameters in creating a NQR-specific watermark is the amplitude of the echo spectrum. As the amplitude is directly proportional to the amount of tag, we can vary the amplitude by modifying the amount. We used L-histidine as an extrinsic tag to differentiate between two samples of common sugar for this proof-of-concept experiment. The tag accounted for 30% and 40%, respectively, of the entire mass of the two samples under test. As shown in Fig. 15, we can use this method to reliably differentiate one extrinsic tag from another; the cross validation accuracy is 100%.

B. *Multiple extrinsic tags*

We can also use multiple NQR-sensitive compounds which are non-reactive both with each other and the actual substance as extrinsic tags. This increases the complexity of the tag and makes it harder to clone. In a proof-of-concept experiment, we used two directly consumable dietary supplements (L-histidine and L-proline) as extrinsic tags in a single sample of infant formula (milk powder) and created a watermark for it. The first sample contained 30% and 40%, respectively, of tagging material by mass, while the second contained 20% and 50%. Fig. 16 shows that we can reliably distinguish between these two cases even though they have the same total amount of tagging material.

As explained in the previous sections, we generally use three parameters per NQR line. For extrinsic tags containing a single compound, we can modify the signal amplitude (A) but not the decay time ($T_{2,eff}$) or linewidth (Δf), because the latter are tag-specific parameters. It can however be argued that the linewidth can be modified and used for extrinsic tagging by using multiple brands of the same compound (i.e., from different manufacturers). However, these changes are small enough that mixtures of multiple brands cannot be resolved using the current apparatus. As a result, they do not enhance security relative to a single-brand tag.

C. *Miscellaneous Effects*

There are several other effects that determine the complexity of extrinsic tags. Firstly, each NQR-sensitive nucleus with spin $I = 1$, such as ^{14}N, generates three resonant lines (see Fig. 2), resulting in up to $3 \times 3 = 9$ classification parameters. However, the lowest-frequency resonance (the ω_0 transition shown in Fig. 2) generally does not have enough sensitivity to be useful, which reduces the number of useful parameters to 6. For example, the single ^{14}N nucleus of acetaminophen has resonances at 2.564, 1.921, and 0.643 MHz. Fig. 17 confirms that the parameters of the first two resonances are distinct.

Secondly, a compound with $N > 1$ NQR-sensitive nuclei will generate an independent set of lines for each nucleus, resulting in $6N$ classification parameters. For example, melamine has $N = 6$ ^{14}N nuclei, and thus has as many as 36 classification parameters. Finally, many compounds have $K > 1$ polymorphic forms, each of which can also generate significantly different NQR parameters. In this case, the number of available parameters increases to $6NK$. Thus, one can greatly increase the complexity of the tag by picking the right tagging compound.

The manufacturing process can also add complexity to extrinsic tags. As explained earlier, the NQR linewidth for pills can vary significantly with pressure applied during manufacturing. Similarly, other physical variables, such as stress, can affect the NQR parameters, hence, the watermark. As an example, we performed an experiment with two samples from the same manufacturer that have the same chemical composition and mass but different physical forms. In particular, both samples contain 500 mg Tylenol (acetaminophen) per pill, but the first consists of regular caplets while the second consists of gelatin capsules (gelcaps). The cross validation accuracy for classifying these samples is high (97%) as shown in Fig. 18.

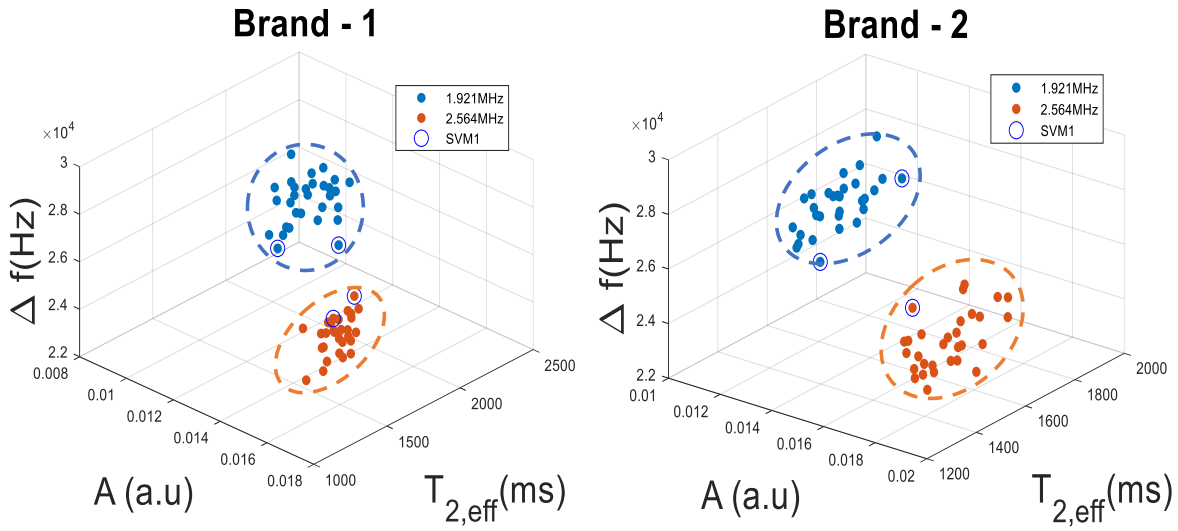

Fig. 17: NQR signatures for two different NQR resonances of the same ^{14}N nucleus in a sample of acetaminophen. Experimental conditions: RF frequency = 2.564 MHz; 1.921 MHz, inter-experimental delay = 3000 ms, pulse length = 200 μs, echo period = 1200 μs, number of echoes = 2048, number of scans = 16, number of pills = 50 (500 mg each).

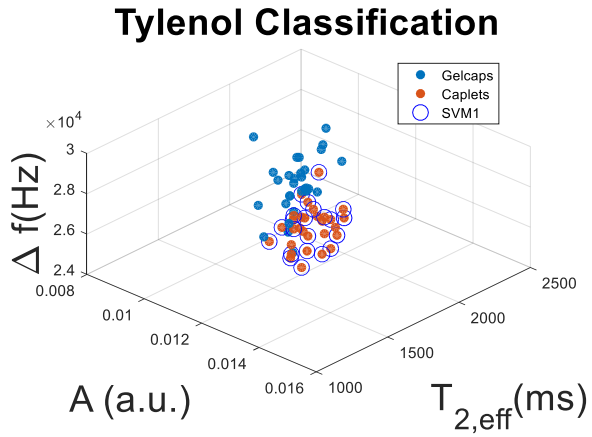

Fig. 18: Classification of two samples of acetaminophen (Tylenol) in (i) caplet form, and (ii) gelcap form. Experimental conditions: RF frequency = 2.564 MHz, inter-experimental delay = 3000 ms, pulse length = 200 μs, echo period = 1200 μs, number of echoes = 2048, number of scans = 16, number of pills = 50 (500 mg each).

D. Randomness Function

The unclonability of an extrinsic tag is vital for ensuring resistance to brute-force attacks. The following equation provides an estimate for the randomness of a tag:

$$\Re = \prod_{\alpha=1}^{K} \prod_{\beta=1}^{2N} \left(\frac{\Delta \mathcal{A}_\beta}{\mathcal{A}_{\beta,sen}} \right) \left(\frac{\Delta \mathcal{L}_\beta}{\mathcal{L}_{\beta,sen}} \right) \left(\frac{\Delta T_\beta}{T_{\beta,sen}} \right), \quad (8)$$

where $\Re$ is the randomness function, K is the number of NQR-sensitive compounds (or polymorphs) used to make an extrinsic tag, and N is the number of NQR-sensitive nuclei (assumed to have spin $I = 1$) inside each compound. As each nucleus has different resonant frequencies, randomness increases exponentially with the total number of nuclei. Moreover, $\Delta \mathcal{A}_\beta$ is the available range of signal amplitudes for a particular nucleus, while $\mathcal{A}_{\beta,sen}$ is the measurement sensitivity, i.e., the smallest detectable change in signal amplitude. Similarly $\Delta \mathcal{L}_\beta$ and ΔT_β are the available ranges of linewidths and decay time constants for that nucleus, respectively, and $\mathcal{L}_{\beta,sen}$ and $T_{\beta,sen}$ are the corresponding sensitivities.

As an example, when three different compounds are used to make a single watermark, then $K = 3$. If each compound has five NQR-sensitive atoms, then $N = 5$. Assuming reasonable values for $\Delta \mathcal{A}_\beta = 10$ gm and $\mathcal{A}_{\beta,sen} = 0.5$ gm, the first term in eqn. (8) is equal to 20. Similarly, assuming $\Delta \mathcal{L}_\beta = 30$ kHz and $\mathcal{L}_{\beta,sen} = 1$ kHz, the second term is equal to 30. Finally, assuming $\Delta T_\beta = 2000$ ms and $\Delta T_\beta = 5$ ms, the third term is equal to 400. Thus, considering all the possible parameter values for this complex extrinsic tag, the randomness function will have a value of $\Re = 2.55 \times 10^{161}$. This result proves that such a three-component extrinsic tag is highly random and quite difficult to estimate using brute force.

VI. Results and Discussion

We have shown that the intrinsic properties of NQR-sensitive nuclei can be utilized to make unique chemical signatures that are highly sensitive to changes in the chemical environment (e.g., due to the manufacturing process, physical structure, etc.). Thus, in some cases they can even be used to differentiate between nominally-identical chemicals from various manufacturers [19]. We have used SVMs with ECOC support vectors to accurately classify different NQR-sensitive substances based on these signatures with relatively low computational complexity. However, not all consumables are NQR-sensitive. In these cases, we proposed an extrinsic tagging approach based on adding consumable NQR-sensitive compounds (see Table II). Compounds with higher NQR resonance frequencies are desirable for such extrinsic tags since

they have higher sensitivity, thus minimizing the amount of tagging material that needs to be added. Methods to optimize sensitivity and SNR per unit time were further discussed in Section IV. The desired complexity of an extrinsic tag depends on the security requirements of a particular product. Simple tags can be made by merely changing the quantity of active ingredient (see Fig. 15). More secure tags can be made by using multiple NQR-sensitive elements (see Fig. 16) or multiple NQR-sensitive nuclei (see Fig. 17). Thus, tag complexity can be varied depending on the application, as described in Section V. Finally, we provided a theoretical analysis of the randomness function of such tags (see eqn. 8) that confirms their highly unclonable nature and thus validates the proposed extrinsic tagging concept.

The existing experimental setup is a bench-top device that consists of a probe, spectrometer, computer, and batteries. This type of device is suitable for industrial authentication applications (e.g., in supply chain management) but is too large and expensive for use by average consumers. In order to address this issue, future work will concentrate on i) miniaturizing the device by replacing the expensive bench-top spectrometer with a system-on-module (SoM); ii) improving sensitivity by using pre-polarization techniques; and iii) reducing local processing requirements by transferring computations to the cloud. Moreover, the current applications of the proposed technique are limited to consumables. Future work will explore additional applications, such as the authentication of common non-consumables like plastics, glass, and metals.

VII. Conclusion

We have presented a novel non-invasive approach for verifying the integrity of consumables and tracing them through a supply chain using chemical tags. Our approach is based on verifying intrinsic chemical and structural properties of NQR-sensitive elements, which can be used as extrinsic tags in diverse products. In particular, we have described how to classify and track consumables by using extrinsic tags that generate unique watermark based on three NQR parameters (amplitude, decay time, and line width). We have demonstrated that these parameters can be measured by a portable authentication device. The proposed approach enables reliable track-and-trace of consumables through the supply chain based on training a machine learning model with measured NQR signatures. Such tags themselves should be safe to consume, e.g., made out of inactive ingredients of a pharmaceutical/supplement product, or additives of a food product. Further, they should be hard-to-clone, which is achievable since the exact watermarks rely on multiple hard-to-replicate manufacturing parameters. We have presented an estimate of the unclonability of these signatures by defining an appropriate randomness function.

Both authentication and unclonability can be further improved by using improved instrumentation that provides higher sensitivity. For example, a pre-polarization system can be added to the existing setup, which uses cross-polarization from protons in a static magnetic field to increase NQR signal amplitude, thereby improving SNR. Our current experimental setup is also limited to solid tags, since NQR is a solid-state technique. In order to extend our approach to a wider set of tags, including liquid, we plan to combine NQR with low-field NMR in our future work. We also plan to explore ways to significantly reduce the amount of tag by using compounds with higher resonance frequencies. Finally, we plan to incorporate extrinsic tags in non-consumables to improve their security using similar authentication approach.

Acknowledgment

This project is sponsored by the National Science Foundation (NSF) under grants SHF-1563688 and SHF-1563924.

References

[1] PWC. (2016) Fighting $40bn food fraud to protect food supply. [Online]. Available: https://press.pwc.com/News-releases/fighting–40bn-food-fraud-to-protect-food-supply/s/44fd6210-10f7-46c7-8431-e55983286e22

[2] E. D. Kantor, C. D. Rehm, M. Du, E. White, and E. L. Giovannucci, "Trends in dietary supplement use among US adults from 1999-2012," *Jama*, vol. 316, no. 14, pp. 1464–1474, 2016.

[3] Z. M. Research. (2017) Global dietary supplements market is expected to reach around USD 220.3 billion in 2022. [Online]. Available: https://www.zionmarketresearch.com/news/dietary-supplements-market

[4] R. J. Maughan, "Contamination of dietary supplements and positive drug tests in sport," *Journal of sports sciences*, vol. 23, no. 9, pp. 883–889, 2005.

[5] FDA. Dietary supplements: What you need to know. [Online]. Available: https://www.fda.gov/Food/DietarySupplements /UsingDietarySupplements/ucm109760.htm

[6] WHO. (2017) 1 in 10 medical products in developing countries is substandard or falsified. [Online]. Available: http://www.who.int/mediacentre/news/releases/2017/substandard-falsified-products/en/

[7] A. Jahnke. (2017) Bad medicine. [Online]. Available: https://www.bu.edu/bostonia/summer17 /bad-medicine/

[8] EUROPOL. (2016) Largest-ever seizures of fake food and drink in interpol-europol operation. [Online]. Available: https://www.europol.europa.eu/newsroom/news/largest-ever-seizures-of-fake-food-and-drink-in-interpol-europol-operation

[9] J. Latosinska, P. Mazurek, and B. Nogaj, "NQR spectroscopy in definition of biological activity of medicines and pesticides," *Materials presented at the 27 All-Polish Seminar on the Nuclear Magnetic Resonance and its application*, 1995.

[10] S. Prez, L. Cerioni, A. Wolfenson, S. Faudone, and S. Cuffini, "Utilization of pure nuclear quadrupole resonance spectroscopy for the study of pharmaceutical crystal forms," *International Journal of Pharmaceutics*, vol. 298, no. 1, pp. 143 – 152, 2005.

[11] J. Latosiska, "Nuclear quadrupole resonance spectroscopy in studies of biologically active molecular systems a review," *Journal of Pharmaceutical and Biomedical Analysis*, vol. 38, no. 4, pp. 577 – 587, 2005.

[12] B. H. Suits, "Nuclear quadrupole resonance spectroscopy," *Handbook of Applied Solid State Spectroscopy*, pp. 65–96, 2006.

[13] Y. Lee, "Spin-1 nuclear quadrupole resonance theory with comparisons to nuclear magnetic resonance," *Concepts in Magnetic Resonance*, vol. 14, no. 3, pp. 155–171, 2002.

[14] J. Barras, K. Althoefer, M. D. Rowe, I. J. Poplett, and J. A. S. Smith, "The emerging field of medicines authentication by nuclear quadrupole resonance spectroscopy," *Applied Magnetic Resonance*, vol. 43, no. 4, pp. 511–529, Dec 2012.

[15] J. Barras, A. Jakobsson, E. Gudmundson, M. D. Rowe, I. J. F. Poplett, J. Luznik, V. Jazbinsek, J. Pirnat, J. Seliger, Z. Trontelj, J. A. S. Smith, and K. Althoefer, *Counterfeit Medicines Volume II: Detection, Identification and Analysis*. Hertfordshire, U.K.: ILM Publications, 2012, ch. The emerging field of medicines authentication by nuclear quadrupole resonance spectroscopy.

[16] J. Barras, D. Murnane, K. Althoefer, S. Assi, M. D. Rowe, I. J. F. Poplett, G. Kyriakidou, and J. A. S. Smith, "Nitrogen-14 nuclear quadrupole resonance spectroscopy: A promising analytical methodology for medicines authentication and counterfeit antimalarial analysis," *Analytical Chemistry*, vol. 85, no. 5, pp. 2746–2753, 2013, pMID: 23384229.

[17] C. Chen, F. Zhang, J. Barras, K. Althoefer, S. Bhunia, and S. Mandal, "Authentication of medicines using nuclear quadrupole resonance spectroscopy," *IEEE/ACM Transactions on Computational Biology and Bioinformatics (TCBB)*, vol. 13, no. 3, pp. 417–430, 2016.

[18] C. Chen, F. Zhang, S. Bhunia, and S. Mandal, "Broadband quantitative NQR for authentication of vitamins and dietary supplements," *Journal of Magnetic Resonance*, vol. 278, pp. 67–79, 2017.

[19] N. V. R. Masna, F. Zhang, C. Chen, S. Mandal, and S. Bhunia, "Authentication of dietary supplements through nuclear quadrupole resonance (NQR) spectroscopy," *International Journal of Food Science & Technology*.

[20] F. Zhang, N. V. Masna, S. Bhunia, C. Chen, and S. Mandal, "Authentication and traceability of food products through the supply chain using NQR spectroscopy," in *Biomedical Circuits and Systems Conference (BioCAS), 2017 IEEE*. IEEE, 2017, pp. 1–4.

[21] D. O. Walsh, "Multi-channel surface NMR instrumentation and software for 1D/2D groundwater investigations," *Journal of Applied Geophysics*, vol. 66, no. 3-4, pp. 140–150, 2008.

[22] T. Leeper. Permutation tests. [Online]. Available: https://thomasleeper.com/Rcourse/Tutorials/permutationtests.html

[23] J. Lužnik, J. Pirnat, V. Jazbinšek, Z. Lavrič, S. Srčič, and Z. Trontelj, "The influence of pressure in paracetamol tablet compaction on 14N nuclear quadrupole resonance signal," *Applied Magnetic Resonance*, vol. 44, no. 6, pp. 735–743, 2013.

[24] G. Kyriakidou, A. Jakobsson, K. Althoefer, and J. Barras, "Batch-specific discrimination using nuclear quadrupole resonance spectroscopy," *Analytical chemistry*, vol. 87, no. 7, pp. 3806–3811, 2015.

[25] C. Jing and V. W. Cornish, "Chemical tags for labeling proteins inside living cells," *Accounts of chemical research*, vol. 44, no. 9, pp. 784–792, 2011.

[26] H. Yu, C.-M. Tang, and R. Bashirullah, "An asymmetric rf tagging ic for ingestible medication compliance capsules," in *Radio Frequency Integrated Circuits Symposium, 2009. RFIC 2009. IEEE*. IEEE, 2009, pp. 101–104.

[27] FDA. Direct food substances affirmed as generally recognized as safe. [Online]. Available: https://www.fda.gov/Food/IngredientsPackagingLabeling/GRAS/

[28] C.-C. Chang and C.-J. Lin, "Libsvm: a library for support vector machines," *ACM transactions on intelligent systems and technology (TIST)*, vol. 2, no. 3, p. 27, 2011.

[29] L. Bottou and C.-J. Lin, "Support vector machine solvers," *Large scale kernel machines*, vol. 3, no. 1, pp. 301–320, 2007.